



Published in final edited form as:

*Lab Chip*. 2012 October 21; 12(20): 3976–3982. doi:10.1039/c2lc40345e.

## A mini-microscope for *in situ* monitoring of cells<sup>†,‡</sup>

Sang Bok Kim<sup>a,b,c</sup>, Kyo-in Koo<sup>a,b,c</sup>, Hojae Bae<sup>a,b,d</sup>, Mehmet R. Dokmeci<sup>a,b</sup>, Geraldine A. Hamilton<sup>c</sup>, Anthony Bahinski<sup>c</sup>, Sun Min Kim<sup>e</sup>, Donald E. Ingber<sup>c,f</sup>, and Ali Khademhosseini<sup>a,b,c</sup>

Ali Khademhosseini: [alik@rics.bwh.harvard.edu](mailto:alik@rics.bwh.harvard.edu)

<sup>a</sup>Center for Biomedical Engineering, Department of Medicine, Brigham and Women's Hospital, Harvard Medical School, Boston, MA, 02115, USA

<sup>b</sup>Harvard-MIT Division of Health Sciences and Technology, Massachusetts Institute of Technology, Cambridge, MA, 02139, USA

<sup>c</sup>Wyss Institute for Biologically Inspired Engineering at Harvard University, Boston, MA, 02115, USA

<sup>e</sup>Department of Mechanical Engineering, Inha University, Incheon, 402-751, Republic of Korea

<sup>f</sup>Vascular Biology, Children's Hospital, Harvard Medical School, Boston, MA, 02115, USA, and Harvard School of Engineering and Applied Sciences, Cambridge, MA, 02138, USA

### Abstract

A mini-microscope was developed for *in situ* monitoring of cells by modifying off-the-shelf components of a commercial webcam. The mini-microscope consists of a CMOS imaging module, a small plastic lens and a white LED illumination source. The CMOS imaging module was connected to a laptop computer through a USB port for image acquisition and analysis. Due to its compact size, 8 × 10 × 9 cm, the present microscope is portable and can easily fit inside a conventional incubator, and enables real-time monitoring of cellular behaviour. Moreover, the mini-microscope can be used for imaging cells in conventional cell culture flasks, such as Petri dishes and multi-well plates. To demonstrate the operation of the mini-microscope, we monitored the cellular migration of mouse 3T3 fibroblasts in a scratch assay in medium containing three different concentrations of fetal bovine serum (5, 10, and 20%) and demonstrated differential responses depending on serum levels. In addition, we seeded embryonic stem cells inside poly(ethylene glycol) microwells and monitored the formation of stem cell aggregates in real time using the mini-microscope. Furthermore, we also combined a lab-on-a-chip microfluidic device for microdroplet generation and analysis with the mini-microscope and observed the formation of droplets under different flow conditions. Given its cost effectiveness, robust imaging and portability, the presented platform may be useful for a range of applications for real-time cellular imaging using lab-on-a-chip devices at low cost.

---

<sup>†</sup>Electronic supplementary information (ESI) available: Supplementary movies for cellular migration in a scratch assay, cell aggregate formation in a microwell, microdroplet generation inside a microfluidic chip and MATLAB code for image capture. See DOI: 10.1039/c2lc40345e

<sup>‡</sup>Published as part of a themed issue dedicated to Emerging Investigators

Correspondence to: Ali Khademhosseini, [alik@rics.bwh.harvard.edu](mailto:alik@rics.bwh.harvard.edu).

<sup>d</sup>Current Address, Department of Maxillofacial Biomedical Engineering and Institute of Oral Biology, School of Dentistry, Kyung Hee University, South Korea

## Introduction

The light microscope is an invaluable tool for cell biology and it has been improved over time to meet different optical imaging demands.<sup>1</sup> For example, phase contrast microscopy has been developed to image a low-contrast objects, such as live cells which can not be seen clearly using a bright-field microscope. The phase contrast microscopy uses an annular phase ring that transforms small phase differences to amplitude differences which enables live cell imaging. Polarization microscopy utilizes polarized light to observe ordered molecules such as spindle fibers and actin filament bundles in living cells. Differential interference contrast (DIC) microscopy is yet another technique that uses dual-beam interference optics for applications demanding high resolution and contrast for inspection of cultured cells.<sup>1</sup> Few efforts have focused on scaling down the size of a light microscope, but because of the development of cell-based lab-on-a-chip applications, this is now an important goal. In biology, many cellular processes, including embryonic development, wound healing and disease progression occur over extended periods of time. Hence, it is beneficial to continuously monitor the state of cells during these processes. The current practice for monitoring of cells in culture requires users to remove the cells from the incubator and inspect them under a microscope. This process not only introduces an added disturbance to cells in culture, but it is also prone to microbial contamination during cell handling. Furthermore, for many lab-on-a-chip applications, this requires detachment of the system from syringe pumps and exposure to numerous subsequent deleterious effects, such as the introduction of bubbles.<sup>2</sup> One possible remedy for observation of cells during culture is to build an incubator around a conventional microscope, an approach which results in bulky and expensive systems. The availability of a miniaturized microscope that can be placed inside an incubator will alleviate most of these problems.

Recently, with the availability of low-cost, compact and high-performance image sensors, such as charge coupled devices (CCDs) and complementary metal oxide semiconductors (CMOS), numerous compact lens-free imaging systems have been reported. In a lens-free imaging system, the diffracted or holographic image of objects are recorded directly onto an image sensor and the real image of the object is usually reconstructed numerically.<sup>3-8</sup> Since lens-free imaging systems do not require any bulky lens systems, they are cost-effective, light-weight and portable. Due to these attractive features, lens-free imaging technology is finding novel applications in biomedical sciences. For example, by using a lens-free imaging system, an ultra wide-field cell detection system has been developed by analyzing the diffraction signature of different cells.<sup>5,6,9</sup> Also, a lens-free cardiotoxicity screening system was recently reported to monitor the beating rates and beat-to-beat variations of cardiomyocytes induced by different drugs in real-time.<sup>10</sup> Furthermore, by using a holographic technique with an improved numerical algorithm, a lens-free imaging system with sub-pixel resolution was introduced,<sup>4,7,11,12</sup> and a lens-free optical tomographic microscope has been developed for three-dimensional (3D) microscopy applications.<sup>13,14</sup>

Despite its compact size, a lens-free imaging system has drawbacks for *in situ* cell monitoring because the object has to be placed close to the image sensor (~100  $\mu\text{m}$ ), which is less than the thickness (~2 mm) of the most common cell culture substrates (*e.g.*, flasks, multi-well plates and Petri dishes). This problem can be resolved using a multi-angle illumination scheme, however, the distance between the object and the image sensor has to be less than 1.1 mm.<sup>15</sup> Recently, an ePetri dish has been reported, which uses an image sensor as the cell culture substrate.<sup>16</sup> The ePetri dish has been applied for long-term observation of cellular behavior, but it still needs numerical reconstruction to obtain images of cells.

Several miniaturized microscopes have been commercialized. Examples include IncuCyte™ (Essen BioScience, Inc.) and LumaScope (Etaluma, Inc.). These microscopes can image cellular behavior inside an incubator but are still expensive and hard to construct by the user. In this study, we used a different approach to develop an inexpensive microscope for *in situ* live cell monitoring by modifying a commercial webcam. This mini-microscope is constructed by combining a compact CMOS imaging sensor with a simple lens that enables objects to be observed without numerical reconstruction. The developed mini-microscope is easy-to-fabricate, highly cost-effective and compact. Due to its compactness, the mini-microscope can be easily placed and used inside a conventional incubator. To demonstrate the versatility of the mini-microscope, we used this instrument to carry out long-term observations of mouse 3T3 fibroblast cells that were undergoing migration in a scratch assay; we also successfully monitored and recorded the formation of mouse embryonic stem cell (ESC) aggregates *in vitro*. In addition, we observed the generation of droplets in a microfluidic device in real-time using the mini-microscope.

## Materials and methods

All cell culture materials were purchased from Invitrogen (USA), unless otherwise specified. In all experiments, the cells were cultured and monitored continuously in a conventional incubator maintained at 37 °C and 5% CO<sub>2</sub>.

### Construction of the mini-microscope

A CMOS imaging module and a plastic lens from a commercial webcam (Logitech, c160) were utilized to construct the mini-microscope. The objective lens of the mini-microscope was fabricated using a 1.5 mL Eppendorf tube. We removed the lid of the Eppendorf tube and cut the closed end to prepare the lens housing. Next, we extracted the plastic lens from the webcam and inserted it inside the housing, and then placed the housing onto the CMOS imager. In a conventional webcam, the lens is used to demagnify the objects, however in our case it was reversed and was used for magnification. The distance between the lens and the image sensor (*i.e.* length of the housing) determined the magnification (Fig. 1). Two plastic housings that were 4 mm and 18 mm in length were prepared and utilized in our experiments to provide a range of magnification.

The main frame of the mini-microscope was constructed using glass slides. The dimensions of the entire microscope were 8 cm (width) × 10 cm (depth) × 9 cm (height) and it was designed in a similar way to an inverted microscope so that conventional cell culture equipment can be placed on top for monitoring cells. A white light-emitting diode (LED) was used as the illumination source (Fig. 1).

The CMOS imaging module was connected to a laptop computer through a USB port. To automate the operations (*i.e.* image capture and image processing), we developed a computer program using MATLAB software (MathWorks, Inc.). The code is flexible and allows the user to select the time intervals between each image capture (see also ESI, text S1†).

### Cell culture, scratch assay and cell fixation

Mouse 3T3 fibroblast cells were cultured in Dulbecco's Modified Eagle's Medium (DMEM) supplemented with 100 units mL<sup>-1</sup> of penicillin/streptomycin (Gibco) and three different concentrations (5, 10, and 20%) of fetal bovine serum (FBS, Atlas). The 3T3 cells were passaged every 3 days. The cells were seeded in a 6-well plate (6 × 10<sup>5</sup> cells per well) and cultured for one day to obtain a confluent cell monolayer. The scratch assay was carried out by scratching the monolayer with a 200 μL pipette tip so that a ring shaped region free of

cells was formed (see Fig. 2). Cell migration into the wound was then monitored using the mini-microscope.

To characterize the mini-microscope's imaging capabilities, the cells were fixed, and the images were captured and compared using both (i) the mini-microscope and (ii) a conventional light microscope. After removing the culture medium, the cells were washed twice using Dulbecco's Phosphate Buffered Saline (DPBS, Gibco) and fixed using 2.5% glutaraldehyde solution (Sigma) for 10 min. The fixed cells were dehydrated in a series of ethanol solutions (70%, 90%, 95% and 100%) for 5 min each. The last dehydration step with 100% ethanol solution was repeated three times. To dry, the fixed cells were placed in a laminar fume hood with hexamethyldisilazane (HMDS) solution (98%, Sigma) for 10 min.

### ESCs culture and cell aggregate formation

Mouse ESCs (R1 cell line) were cultured in DMEM supplemented with 2 mM of L-glutamine, 100 units  $\text{mL}^{-1}$  penicillin/streptomycin, 0.1 mM  $\beta$ -mercaptoethanol, 1000 units  $\text{mL}^{-1}$  leukemia inhibitory factor (LIF, Chemicon) and 10% of ESC qualified fetal bovine serum (ES-FBS). The medium was changed daily. ESCs were passaged before reaching 70% confluence. To generate ESC aggregates, poly(ethylene glycol) (PEG) micro-wells were utilized.<sup>17</sup> ESCs were seeded inside the PEG microwells and cultured in alpha Minimum Essential Medium ( $\alpha$ -MEM) supplemented with 15% heat inactivated fetal bovine serum (HI-FBS) and 100 units  $\text{mL}^{-1}$  penicillin/streptomycin. Since the ESCs do not adhere to the surface of the PEG microwells, they aggregated and formed spherical structures which were monitored using the mini-microscope for 18 h

### Microfluidic device for microdroplet generation and analysis

A poly(dimethylsiloxane) (PDMS, Sylgard 184, Dow Corning) lab-on-a-chip microfluidic device was fabricated using standard soft lithography to generate microdroplets.<sup>18</sup> The microfluidic device had two microchannels, which intersect each other in a perpendicular manner. Each microchannel had a square cross-section ( $150 \mu\text{m} \times 100 \mu\text{m}$ ). Water and mineral oil were introduced to the main and side channels, respectively. The flow rates of water and mineral oil were controlled using a syringe pump (PHD 2000, Harvard Apparatus). The flow rate of water was fixed as  $50 \mu\text{l h}^{-1}$ . The formation of water droplets under different flow rates of mineral oil ( $100, 150, 200, 300 \mu\text{l h}^{-1}$ ) was monitored using the mini-microscope.

## Results and discussion

### Characterization of the mini-microscope

**Working distance and focus adjustment**—To measure the working distance (*i.e.* the distance between the sample and the surface of the lens), we placed microspheres on a plate and increased the distance between the microspheres and the lens until a focused image was obtained. The measured working distance of the plastic lens was 4.5 mm. The sample stage of the mini-microscope was designed to maintain an optimum working distance from the lens by stacking glass slides instead of having a focus-adjusting knob. Since the plastic lens has a low numerical aperture (NA), the depth of focus (DOF) of the lens is larger than the DOF of a standard objective lens. Due to the large DOF, we can image samples without a need for fine adjustment in the *z*-axis. However, the low NA limits the resolution as described in following section.

**Magnification and field of view (FOV)**—To demonstrate the optical performance of the mini-microscope, images of fixed mouse 3T3 fibroblasts were recorded using the mini-microscope and compared with those obtained using a conventional light microscope (Fig.

3). Fig. 3A shows an image taken with the mini-microscope with a housing length of 4 mm. For comparison, the images obtained from a light microscope with 4× and 10× objective lens are shown in Fig. 3B and 3C, respectively. We observed that the magnification of the mini-microscope with a 4 mm housing length was comparable to a 10× microscope objective (equivalent to 100× magnification). To obtain higher magnification, we used a longer housing (18 mm). The imaged cells are shown in Fig. 3D. As can be seen, the nuclei of the cells are clearly distinguishable. Comparing Fig. 3D and 3E, we observed that our mini-microscope has a magnification similar to a conventional microscope with a 40× objective (equivalent to 400× magnification). The measured FOVs of 4 and 18 mm housing were  $1.52 \times 1.13$  mm and  $0.21 \times 0.16$  mm, respectively.

**Resolution**—To estimate the resolution of the mini-microscope, microspheres (1.2 μm in diameter) were imaged. The variations in light intensity due to the presence of the microparticles were measured by the CMOS imager. For a single microsphere, full width half maximum (FWHM) of the intensity distribution was 2.05 μm which was larger than the actual size of the microsphere.

We believe that this discrepancy is due to the low NA of the plastic lens. The formal definition of the resolution of a microscope is the ability to distinguish two closely spaced points. Therefore, we next imaged two closely spaced microspheres. As shown in Fig. 3F, the center-to-center distance between two 1.2 μm microspheres was measured to be 1.4 μm. Based on this observation, we concluded that the resolution of the mini-microscope is about 1.4 μm or better. This resolution is lower than that of a conventional light microscope, but is sufficient for observing cells. Moreover, the resolution of the mini-microscope can be improved by using a commercially available aspherical plastic lens with a high NA.

### Evaluation of scratch assay of mouse 3T3 fibroblast cells

The *in vitro* scratch assay is often used to mimic and understand the wound healing process and study cell-cell and cell-extracellular matrix (ECM) interactions that mediate this response.<sup>19</sup> In a scratch assay, an artificial gap (scratch) is generated in a confluent cell monolayer and migration of the remaining cells from the edge of the wound into the scratch area is monitored. Fibroblast cells play a central role in wound repair.<sup>20</sup> Hence, in this study, we first created a scratch assay and then monitored the effects of the concentration of FBS on cellular migration rates of mouse 3T3 fibroblast cells. It is known that serum factor affects the migration of 3T3 cells.<sup>21</sup> In this study, we monitored 3T3 cell migration in media containing three different concentrations of FBS to demonstrate the mini-microscope.

To evaluate the effect of the FBS concentration on cell migration, 3T3 cells were cultured in 6-well plates in media containing three different concentrations of FBS (5, 10, or 20%); FBS used in all experiments was aliquoted from a single bottle (ATLAS) to minimize batch-to-batch variability. First, the cells were cultured for one day to obtain a confluent cell monolayer. Then, using a pipette tip, a ring shaped wound assay was generated in the monolayer. The cells were washed twice in DPBS and re-fed with fresh medium. The 6-well plate containing the cells with the scratch assay was then placed onto the mini-microscope. The images were captured every 2 min for 1000 min. From the sequentially captured images, changes in the scratch area were calculated as a function of time using an edge detection algorithm. All data were obtained from three different measurements.

Fig. 4 shows the captured images and the corresponding reconstructed images using an edge detection scheme after 0, 500, and 1000 min for all three FBS concentrations. After 1000 min, the wound was almost closed in the medium supplemented with 5 or 10% FBS; however, it did not completely close in 20% FBS. To evaluate cell migration rates, the scratch areas measured over time were calculated and plotted in Fig. 5. For all 3 FBS

concentrations, there was a 4 h time delay between the generation of the scratch assay and the start of cell migration into the wound. Fibroblasts are known to respond to wounding by first secreting proteins and synthesizing ECM, prior to migrating into the scratch area.<sup>20</sup> We believe that the 4 h time delay observed in our experiments is related to these processes.

We observed slightly varying cell migration rates in medium with different FBS solutions. To quantify the differences in migration rates, an average migration rate based on 1000 min of monitoring was calculated. First, the image was converted to binary, where the cell occupied pixels were given a value 1 and pixels in scratch area were given the value 0. The variation of the scratch area was calculated by counting the number of zero-valued pixels in the binary images. The average migration rates were found to be  $259 \pm 27.5 \mu\text{m}^2 \text{min}^{-1}$ ,  $252 \pm 8.2 \mu\text{m}^2 \text{min}^{-1}$  and  $212 \pm 7.7 \mu\text{m}^2 \text{min}^{-1}$  for medium loaded with 5%, 10% and 20% FBS concentrations, respectively. For medium containing 5 or 10% FBS, the cell migration rates were not significantly different; however, for the medium with 20% FBS, the migration rate was found to be significantly slower. This is possibly due to the fact that FBS contains not only growth factors but also inhibitors of cell proliferation and migration. Therefore, it may be that there is an optimum concentration of FBS for cell spreading and migration, which was between 5 and 10% in our experiments with these mouse 3T3 fibroblasts.<sup>22</sup>

### Monitoring ESC aggregate formation inside PEG microwells

ESCs, which can be obtained by isolation from the inner cell mass during the blastocyst stage, are characterized by their ability for self-renewal and pluripotency.<sup>23</sup> Due to these properties, studies of ESCs are of great interest for cell-based therapies and tissue engineering.<sup>24,25</sup> It is well known that controlling the microenvironment of ESCs plays a key role in their differentiation.<sup>26,27</sup> This has led to the use of microscale technologies to study ESC biology.<sup>17,28,29</sup> Therefore, *in situ* monitoring of stem cells may help to provide new insight into ESC biology.

To assess the utility of the mini-microscope for visualizing cells in a microengineered culture platform, we monitored the formation of ESC cell aggregates in PEG microwells. ESC aggregates can form embryoid bodies (EBs) that contain all three primary germ layers (endoderm, ectoderm and mesoderm).<sup>25</sup> A recent study showed that the size of the EB can regulate ESC differentiation.<sup>17</sup> To create ESC aggregates, ESCs were first seeded inside a PEG microwell (450  $\mu\text{m}$  in diameter and depth). Next, we placed the PEG microwell containing ESCs on the mini-microscope and monitored the formation of cell aggregates. Fig. 6 shows sequentially captured images during cell aggregate formation. Initially, the ESCs sedimented on the bottom surface of the microwell. Within 12 h, the ESCs started to aggregate and formed floating spheroids (see also ESI Movie S2†). As the ESCs aggregated, they formed dense spherical EBs. With this, we demonstrated that the mini-microscope can not only capture images from conventional cell culture flasks, but also it can be utilized with novel microfabricated culture platform.

### Monitoring the generation of droplets inside a microfluidic chip

Recently, microdroplets in microfluidics have been extensively utilized in chemical and biological applications.<sup>30–33</sup> In contrast to continuous flow, the droplet or digital fluidics further reduce sample volumes (pico- and nano-liter) and enable a range of high throughput studies.<sup>31</sup> The droplets are often generated in microfluidic chips by flow instability due to the induced shear force between two immiscible fluids. During microdroplet generation, *in situ* monitoring is required to find optimum flow conditions for generating droplets with desired shapes and dimensions. *In situ* monitoring also allows for observation of reactions inside droplets.

By using our mini-microscope, we monitored the formation of droplets in real-time. To generate the droplets, we utilized a flow focusing geometry<sup>31</sup> (Fig. 7). Water and mineral oil solutions were simultaneously injected into the center and side channels, respectively. Food dye was dissolved in a water solution to better distinguish the water droplets in oil. The size of the droplets were controlled by adjusting the fluid flow rate ratios ( $Q_{oil}/Q_w$ ). We set the flow rate of water ( $Q_w$ ) to  $50 \mu\text{l h}^{-1}$  and changed the flow rate of oil ( $Q_{oil}$ ) to 100, 150, 200, and  $300 \mu\text{l h}^{-1}$ , and observed the effects of different fluid flow-rate ratios on droplet generation. Fig. 7 shows images of generated droplets captured by the mini-microscope for different fluid flow-rate ratios. The increase in oil flow-rate resulted in a decrease in droplet size due to the higher shear stress, and an increase in the rate of droplet generation (see also ESI Movie S3†).

## Conclusions

A simple method to create a cost-effective and portable mini-microscope was presented. Using a CMOS imager, a plastic lens and an LED, we fabricated a miniature portable mini-microscope of comparable quality to a microscope with a 40× objective. The microscope is compatible with conventional cell culture equipment, such as cell culture flasks, multi-well plates and Petri dishes, as well as microengineered culture platforms, and it can be readily utilized inside a common incubator.

To demonstrate the functionality of the mini-microscope, we conducted three experiments. In the first experiment, we monitored cell-migration rates as a function of FBS concentration, using a scratch assay. In the second experiment, we utilized a PEG microwell platform and monitored the formation of cell aggregates using the mini-microscope in real-time. In the third demonstration, we monitored the influence of different flow conditions to the formation of droplets inside a microchannel. In these demonstrations, the mini-microscope performed as well as a conventional optical microscope, yet was compact and allowed continuous *in situ* monitoring of cellular processes for extended periods of time.

It is important to note that while the mini-microscope is highly functional, further improvements can be made to our system. For example, the plastic lens used in this mini-microscope could easily be replaced with a low-cost plastic aspherical lens with a high numerical aperture so that the resolution and the image quality can be improved. The maximum image-capturing rate of the current mini-microscope is 30 frames per second, which is fast enough to detect squirming cells such as beating cardiomyocytes. The capture rate can also be easily improved by using a high-speed image sensor. Moreover, several mini-microscopes can be operated in parallel, which enables the simultaneous imaging of multiple samples. In addition to live-cell monitoring, the mini-microscope can be a powerful and versatile approach to reduce the current large dimensional gap between state-of-art microscale devices and the observation tools in emerging point-of-care systems.

## Supplementary Material

Refer to Web version on PubMed Central for supplementary material.

## Acknowledgments

This work was supported by the National Institute of Health (U01 NS073474) from the NIH Common Fund, through the Division of Program Coordination, Planning, and Strategic Initiatives (DPCPSI), Office of the Director, NIH, the Food and Drug Administration (FDA), NIH (GM095906), the Wyss Institute for Biologically Inspired Engineering at Harvard University and the National Research Foundation of Korea Grant funded by the Korean Government (NRF-2010-220-D00014).

## References

1. Murphy, DB. Fundamentals of light microscopy and electronic imaging. Wiley-Liss; New York: 2001.
2. Selimovic S, Dokmeci MR, Khademhosseini A. Lab Chip. 2012; 12:1409–1411. [PubMed: 22419032]
3. Mudanyali O, Tseng D, Oh C, Isikman SO, Sencan I, Bishara W, Oztoprak C, Seo S, Khademhosseini B, Ozcan A. Lab Chip. 2010; 10:1417–1428. [PubMed: 20401422]
4. Bishara W, Su TW, Coskun AF, Ozcan A. Opt Express. 2010; 18:11181–11191. [PubMed: 20588977]
5. Seo S, Su TW, Tseng DK, Erlinger A, Ozcan A. Lab Chip. 2009; 9:777–787. [PubMed: 19255659]
6. Kim SJ, Yokokawa R, Leshner-Perez SC, Takayama S. Anal Chem. 2012; 84:1152–1156. [PubMed: 22206453]
7. Cui X, Lee LM, Heng X, Zhong W, Sternberg PW, Psaltis D, Yang C. Proc Natl Acad Sci U S A. 2008; 105:10670–10675. [PubMed: 18663227]
8. Garcia-Sucerquia J, Xu W, Jericho SK, Klages P, Jericho MH, Kreuzer HJ. Appl Opt. 2006; 45:836–850. [PubMed: 16512525]
9. Su TW, Seo S, Erlinger A, Ozcan A. Biotechnol Bioeng. 2009; 102:856–868. [PubMed: 18853435]
10. Kim SB, Bae H, Cha JM, Moon SJ, Dokmeci MR, Cropek DM, Khademhosseini A. Lab Chip. 2011; 11:1801–1807. [PubMed: 21483937]
11. Bishara W, Sikora U, Mudanyali O, Su TW, Yaglidere O, Luckhart S, Ozcan A. Lab Chip. 2011; 11:1276–1279. [PubMed: 21365087]
12. Zheng G, Lee SA, Yang S, Yang C. Lab Chip. 2010; 10:3125–3129. [PubMed: 20877904]
13. Isikman SO, Bishara W, Mavandadi S, Yu FW, Feng S, Lau R, Ozcan A. Proc Natl Acad Sci U S A. 2011; 108:7296–7301. [PubMed: 21504943]
14. Isikman SO, Bishara W, Sikora U, Yaglidere O, Yeah J, Ozcan A. Lab Chip. 2011; 11:2222–2230. [PubMed: 21573311]
15. Su TW, Isikman SO, Bishara W, Tseng D, Erlinger A, Ozcan A. Opt Express. 2010; 18:9690–9711. [PubMed: 20588819]
16. Zheng G, Lee SA, Antebi Y, Elowitz MB, Yang C. Proc Natl Acad Sci U S A. 2011; 108:16889–16894. [PubMed: 21969539]
17. Hwang YS, Chung BG, Ortmann D, Hattori N, Moeller HC, Khademhosseini A. Proc Natl Acad Sci U S A. 2009; 106:16978–16983. [PubMed: 19805103]
18. Selimovic S, Sim WY, Kim SB, Jang YH, Lee WG, Khabiry M, Bae H, Jambovane S, Hong JW, Khademhosseini A. Anal Chem. 2011; 83:2020–2028. [PubMed: 21344866]
19. Liang CC, Park AY, Guan JL. Nat Protoc. 2007; 2:329–333. [PubMed: 17406593]
20. Zavan B, Brun P, Vindigni V, Amadori A, Habeler W, Pontisso P, Montemurro D, Abatangelo G, Cortivo R. Biomaterials. 2005; 26:7038–7045. [PubMed: 15993941]
21. Lipton A, Klinger I, Paul D, Holley RW. Proc Natl Acad Sci U S A. 1971; 68:2799–2801. [PubMed: 5288259]
22. Er HM, Cheng EH, Radhakrishnan AK. J Ethnopharmacol. 2007; 113:448–456. [PubMed: 17698306]
23. Blitterswijk, CA; Thomsen, P. ScienceDirect (Online service). Tissue engineering. Elsevier/ Academic Press; Amsterdam; Boston: 2008.
24. Koh CJ, Atala A. J Am Soc Nephrol. 2004; 15:1113–1125. [PubMed: 15100351]
25. Wobus AM, Boheler KR. Physiol Rev. 2005; 85:635–678. [PubMed: 15788707]
26. Postovit LM, Margaryan NV, Seftor EA, Kirschmann DA, Lipavsky A, Wheaton WW, Abbott DE, Seftor RE, Hendrix MJ. Proc Natl Acad Sci U S A. 2008; 105:4329–4334. [PubMed: 18334633]
27. Bratt-Leal AM, Carpenedo RL, McDevitt TC. Biotechnol Prog. 2009; 25:43–51. [PubMed: 19198003]
28. Khademhosseini A, Ferreira L, Blumling J. Biomaterials. 2006; 27:5968–5977. [PubMed: 16901537]

29. Khademhosseini A, Langer R, Borenstein J, Vacanti JP. *Proc Natl Acad Sci U S A*. 2006; 103:2480–2487. [PubMed: 16477028]
30. Hofmann TW, Hanselmann S, Janiesch JW, Rademacher A, Bohm CH. *Lab Chip*. 2012; 12:916–922. [PubMed: 22252585]
31. Theberge AB, Courtois F, Schaerli Y, Fischlechner M, Abell C, Hollfelder F, Huck WT. *Angew Chem, Int Ed Engl*. 2010; 49:5846–5868. [PubMed: 20572214]
32. Huebner A, Sharma S, Srisa-Art M, Hollfelder F, Edel JB, Demello AJ. *Lab Chip*. 2008; 8:1244–1254. [PubMed: 18651063]
33. Huebner A, Olguin LF, Bratton D, Whyte G, Huck WT, de Mello AJ, Edel JB, Abell C, Hollfelder F. *Anal Chem*. 2008; 80:3890–3896. [PubMed: 18399662]

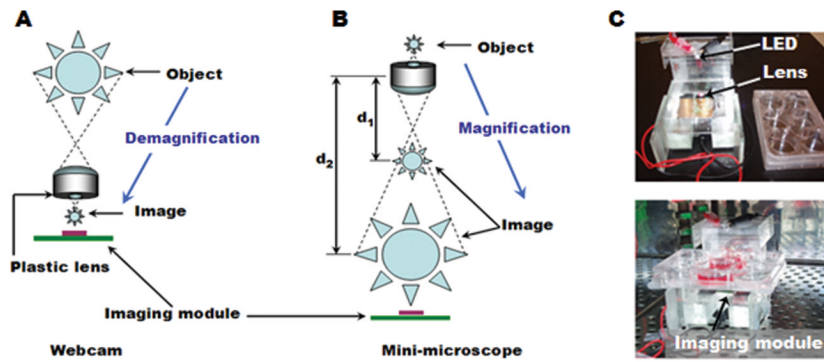


**Fig. 1.** Schematic of the mini-microscope. (A) The role of the plastic lens in a conventional webcam is demagnification of the objects. (B) In the mini-microscope, the plastic lens was reversed and used for magnification. The distance between the imaging module and the lens determines magnification. (C) The mini-microscope is compatible with conventional cell culture equipment and fits easily inside a cell culture incubator for *in situ* cell monitoring.

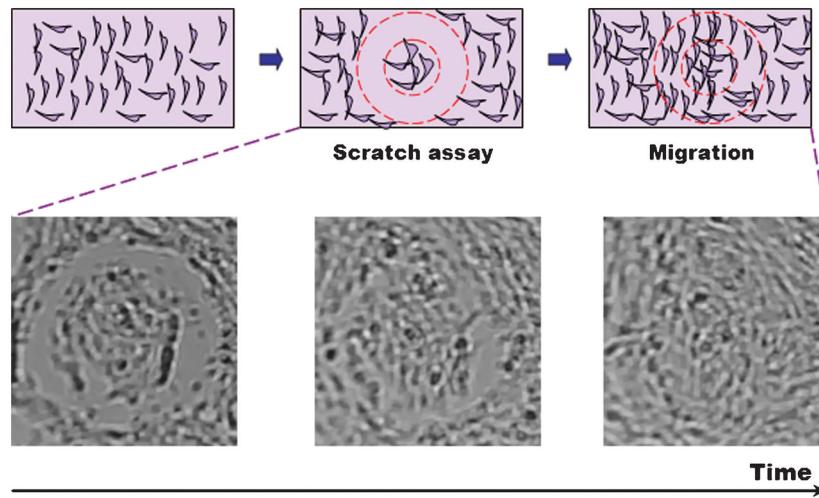


**Fig. 2.** Experimental procedure for creating and monitoring the scratch assay. The mouse 3T3 fibroblast cells were seeded in a 6-well plate and cultured until confluence. A 200  $\mu$ L pipette tip was used to create a scratch assay. The migration of cells towards the scratch area was monitored using the mini-microscope.

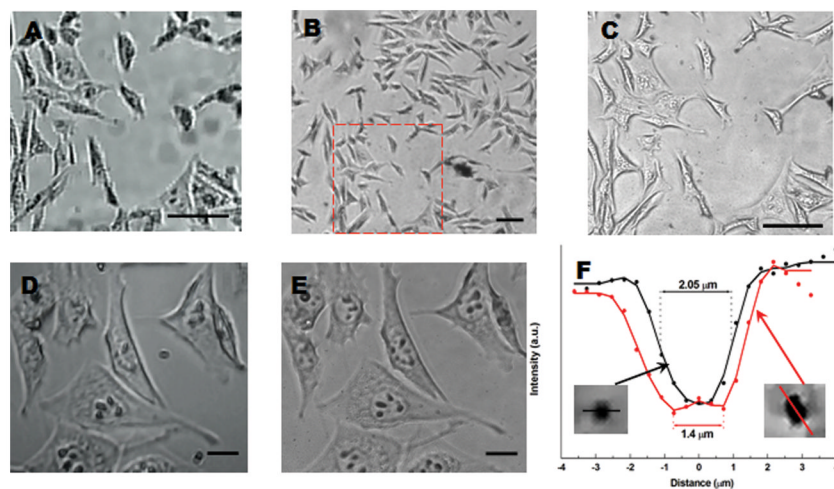


**Fig. 3.**

Comparison of images obtained using the mini-microscope and a conventional light microscope. Images of mouse 3T3 fibroblast cells obtained using the mini-microscope with a housing length of 4 mm (A) and 18 mm (D) and compared with images obtained using a conventional light microscope with 4× (B), 10× (C) and 40× (E) objective lens. To evaluate the resolution of the mini-microscope, the images of 1.2  $\mu\text{m}$  PSL microspheres were captured and analyzed (F). Light intensity distribution on the imager due to a single microsphere (black) and two adjacent microspheres (red). (scale bar: 100  $\mu\text{m}$  (A)–(C), 20  $\mu\text{m}$  (D) and (E)).

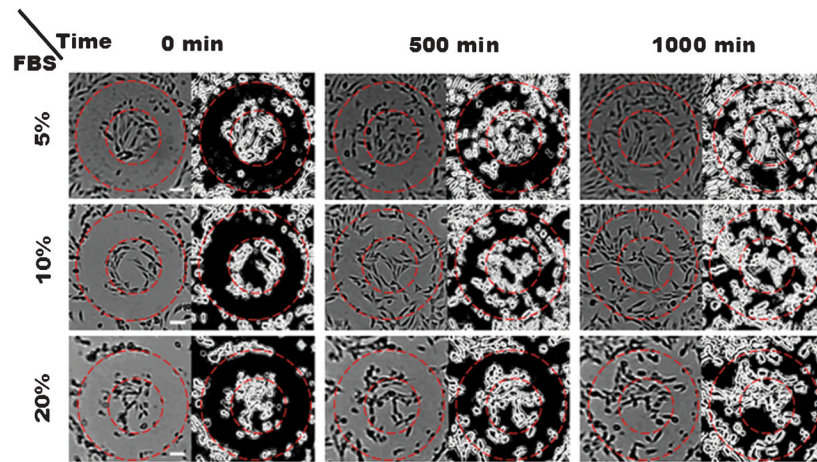


**Fig. 4.** Images captured by the mini-microscope during migration of 3T3 fibroblast cells and the corresponding images obtained using an edge detection algorithm. The red circle shows the initial scratch area. Scale bar: 200  $\mu\text{m}$ . (See also ESI Movie S2).<sup>†</sup>

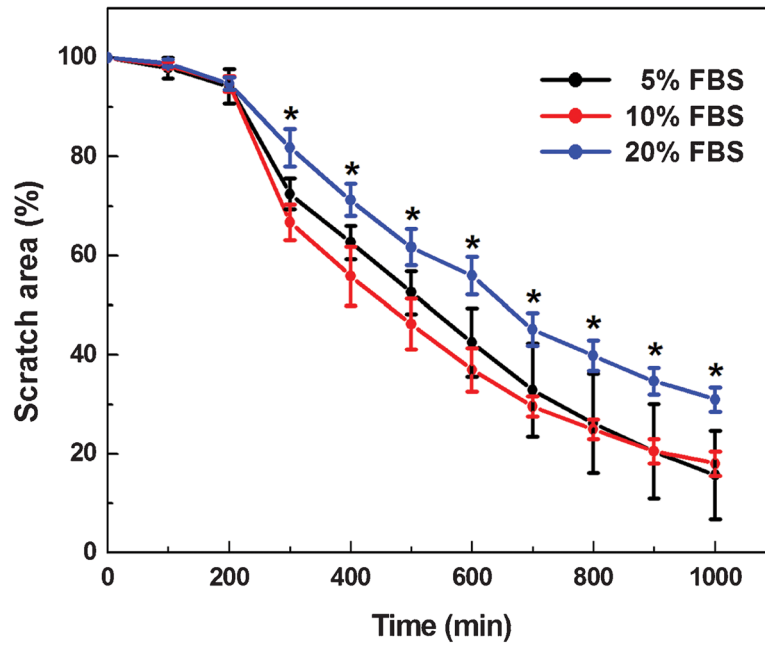


**Fig. 5.** Change in scratch area as a function of time for different FBS concentrations in the culture medium. A 4 h time delay was observed before the cells start to migrate into the scratch area for all concentrations of FBS. \* shows a significant difference in variance ( $p < 0.05$ ). For statistical analysis, one-way ANOVA was used.

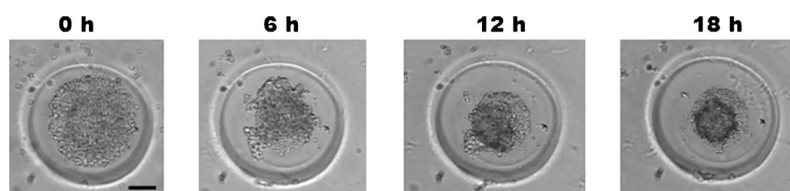


**Fig. 6.** ESC aggregates formation inside a PEG microwell. Mouse ESCs were seeded in a PEG microwell and were monitored using the mini-microscope. ESCs aggregated and formed dense spheroids. After approximately 12 h of seeding, cell aggregates formed and then began to float in the microwell. (See also ESI Movie S3†). Scale bar: 100  $\mu\text{m}$ .

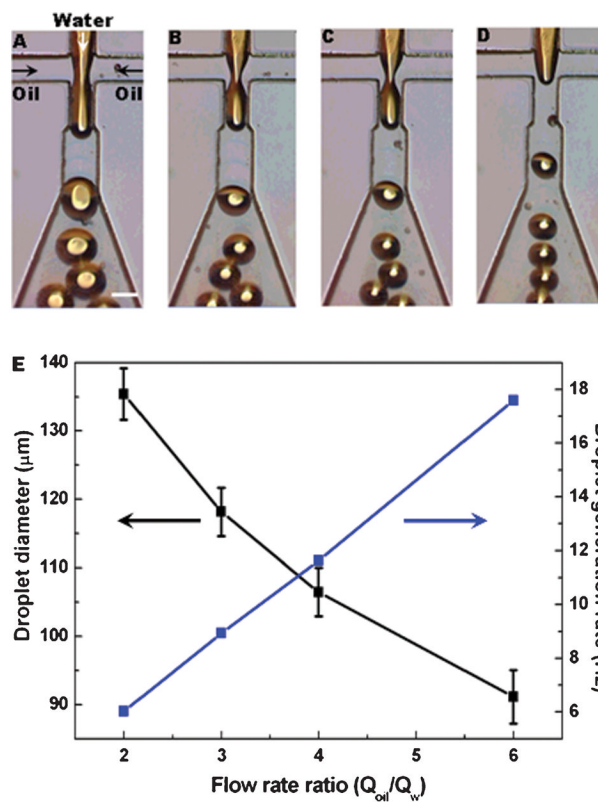


**Fig. 7.** Real-time imaging of microfluidic droplet generation using the mini-microscope. Water droplets were generated with a water flow-rate of  $50 \mu\text{l h}^{-1}$  and an oil flow-rate of  $100 \mu\text{l h}^{-1}$  (A),  $150 \mu\text{l h}^{-1}$  (B),  $200 \mu\text{l h}^{-1}$  (C) and  $300 \mu\text{l h}^{-1}$  (D). Droplet size and droplet generation rate as a function of the fluid flow rate ratio (E). (See also ESI Movie S4†). Scale bar:  $100 \mu\text{m}$ .